Dynamical quantum phase transitions in interacting atomic interferometers

Changyuan Lyu and Qi Zhou

Phys. Rev. A **101**, 043605 — Published 9 April 2020

DOI: 10.1103/PhysRevA.101.043605

Dynamical Quantum Phase Transitions in Interacting Atomic Interferometers

Changyuan Lyu and Qi Zhou*
Department of Physics and Astronomy, Purdue University, West Lafayette, Indiana 47907, USA
(Dated: March 10, 2020)

Particle-wave duality has allowed physicists to establish atomic interferometers as celebrated complements to their optical counterparts in a broad range of quantum devices. In particular, interactions give rise to multi-particle correlations unavailable in linear interferometers. Here, we show that interactions lead to dynamical quantum phase transitions (DQPT) between NOON states in an atomic interferometer. These transition points result from zeros of Loschmidt echo, which approach the real axis of the complex time plane in the large particle number limit, and signify pair condensates, another type of exotic quantum states featured with prevailing two-body correlations. Such DQPTs thus provide us with a new angle to understand many-body states emergent from quantum non-equilibrium dynamics. Our work also suggests interacting atomic interferometers as a new tool for creating highly entangled states to beat the standard quantum limit.

I. INTRODUCTION

Applications of atomic interferometers span a wide spectrum of problems, ranging from measuring the gravitational acceleration and the fine-structure constant to detecting gravitational waves [1–5]. Ultracold atoms prompt a precise control of atomic interferometers, including realizing highly tunable atomic beam splitters [6–10] and accessing an atomic Hong-Ou-Mandel interferometer using optical tweezers [11–14]. Whereas mutual interactions between particles may induce decoherence [15–17], they could also generate squeezing and multi-particle correlations unattainable in linear interferometers [18].

Dynamical quantum phase transition [19–22] has recently invoked enthusiasm in multiple disciplines. A particular type of Loschmidt echo, $|G(t)|^2 = |\langle\psi(0)|\, e^{-\frac{i}{\hbar}\hat{H}t}\, |\psi(0)\rangle|^2$, where $|\psi(0)\rangle$ is the initial state, is considered as the temporal analog of the partition function. When $|\psi(0)\rangle$ is an equal superposition of all energy eigenstates, $|G(t)|^2$ is exactly the partition function with an imaginary temperature $T = \frac{1}{ik_B t}$. t is therefore identified as the tuning parameter as analogous to the temperature in phase transitions at equilibrium. When $G(t) = 0$, the dynamic free energy $\lambda(t) = -\frac{1}{N}\ln|G(t)|^2$, which is the rate function of the probability for the system to return to its initial state, manifests nonanalyticities and defines a critical time t_c. N is the number of degrees of freedom. Similar to conventional phase transitions triggered by Lee-Yang zeros or Fisher zeros in the complex plane of certain parameters or the temperature [23, 24], DQPTs can also be understood from zeros of $G(t)$ in the complex plane by extending the real time t to the complex domain, $t \to z \equiv t + i\tau$. With increasing N, discrete zeros merge to continuous manifolds and eventually touch the real t axis, making physical observables nonanalytic. Whereas observations of DQPTs have been reported in certain spin systems, showing deep connections with equilibrium quantum phase transition and order parameter dynamics [19, 25–30], such novel concept well deserves both theoretical and experimental studies in a much broader range of systems.

In this paper, we show that interacting interferometers host DQPTs between highly entangled quantum states. Starting from a Fock state, pair condensates, which are featured with vanishing one-body correlation and prevailing two-body correlations [31–33], arise in non-equilibrium quantum dynamics. In the large N limit, their appearance at critical times, t_c, are triggered by zeros of $G(z)$ in the complex time plane that approach the real axis, signifying DQPTs at which the many-body wave function becomes orthogonal to the initial state [19, 25, 27–30, 34–36]. t_c characterizes transitions between NOON states, a particular type of Schrodinger's cat states formed by two Fock states. Such dynamically generated NOON states are much more stable than those at equilibrium. The energy mismatch between the two single-particle states only needs to be suppressed as a power-law of N, unlike the equilibrium case where the energy mismatch has to be exponentially small.

Moreover, NOON states arise from an intriguing interplay between interactions and the symmetry. When the Hamiltonian remains unchanged after swapping the two single-particle states, the dynamical phase induced by interactions directly leads to a superposition of the initial state and its counterpart created by the symmetry operator, say $|N, 0\rangle$ and $|0, N\rangle$. Therefore, the NOON states are protected by the symmetry in the sense that any perturbations respecting this symmetry are no longer important. For instance, adding weak multi-particle interactions to the ordinary two-particle interactions does not affect any qualitative results. Thus, our scheme applies to a large class of models and suggests a new mechanism to access highly entangled states, which could be used to beat the standard quantum limit and improve quantum sensing [37–40].

* zhou753@purdue.edu

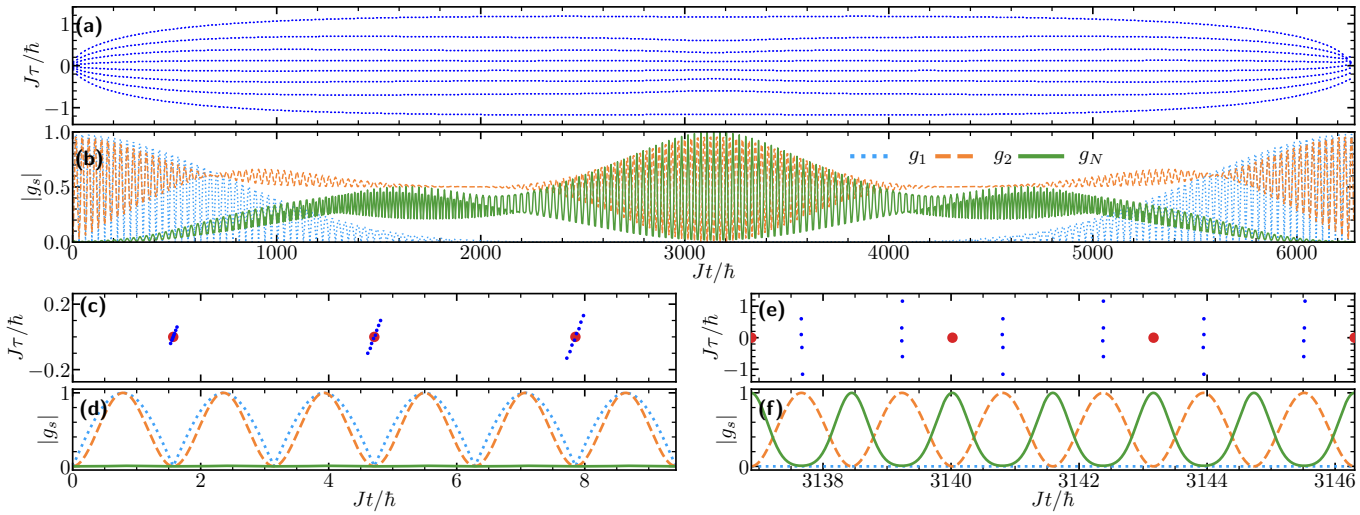

FIG. 1. (color online) Dynamics of 8 bosons for $U/J = 0.001$. (a) Each small blue dot represents a simple zero of $G(z)$ in the complex plane, where z is the complex time $z = t + i\tau$. (b) Normalized s-body correlation $\frac{2|g_1|}{N}, \frac{4|g_2|}{N(N-1)}, \frac{2|g_N|}{N!}$ as functions of the real time t. (c,d) and (e,f): Enlarged regimes of of (a,b) near $t = 0$ and t^*, respectively. Each big red dot in (c,e) are zeros of $G(z)$ of the non-interacting systems described by $z = (k + 1/2)T, k \in \mathbb{Z}$. Each of them has multiplicity 8. The legend in (b) also applies to (d) and (f).

II. HAMILTONIAN

We consider N bosonic atoms in an interferometer consisting of two quantum states. The Hamiltonian reads

$$\hat{H} = -J(\hat{a}_1^\dagger \hat{a}_2 + \hat{a}_2^\dagger \hat{a}_1) + g(\hat{n}_1^2 + \hat{n}_2^2) + 2g_{12}\hat{n}_1\hat{n}_2, \quad (1)$$

where $J > 0$ is the the coupling strength between the two quantum states, $\hat{a}_i^\dagger$ is the creation operator in the ith state, and $\hat{n}_i = \hat{a}_i^\dagger \hat{a}_i$. g and g_{12} are the intra- and inter-state interactions, respectively. This Hamiltonian remains unchanged with two modes swapped. If we consider two spatial modes, this is the inversion symmetry. Though our results apply to generic models respecting this symmetry, we focus on two-particle interactions to concretize discussions. Multi-particle interactions, which may arise from multi-band effects [41], are discussed in Appendix F.

The Hamiltonian can be rewritten as

$$\hat{H} = -J(\hat{a}_1^\dagger \hat{a}_2 + \hat{a}_2^\dagger \hat{a}_1) + \frac{\bar{U}}{2}(\hat{n}_1 + \hat{n}_2)^2 + \frac{U}{4}(\hat{n}_1 - \hat{n}_2)^2, \quad (2)$$

where $\bar{U} = g + g_{12}$, $U = 2(g - g_{12})$. Due to the conservation of the total particle number $N = n_1 + n_2$, $\bar{U}$ only contributes a trivial total phase of the wave function in the dynamics. We thus focus on interaction effects caused by U. Though this Hamiltonian has been well studied [15, 18, 42–46], our results, including zeros of $G(z)$ in the complex time plane, DQPTs, symmetry protected NOON states and pair condensates, elude the literature. We solidify the discussion for repulsive interactions, $U > 0$. Attractive interactions lead to similar results (Appendix B).

III. ZEROS IN THE COMPLEX PLANE.

We consider an initial state, $|\psi(0)\rangle = |N, 0\rangle = \frac{1}{\sqrt{N!}}\hat{a}_1^{\dagger N}|0\rangle$. The dynamical evolution, $|\psi(t)\rangle = e^{-\frac{i}{\hbar}\hat{H}t}|\psi(0)\rangle$, is computed by expanding $|\psi(0)\rangle$ using exact eigenstates of $\hat{H}$. Whereas this can be done for any parameters, we consider $UN^2 \ll J$. Such energy scale separation leads to a time scale separation,

$$T \equiv \frac{\pi\hbar}{J} \ll t^* \equiv \frac{\pi\hbar}{U}, \quad (3)$$

which allows us to access quantum dynamical evolutions exhibiting extraordinary features. When U vanishes, the quantum dynamics is governed by

$$\hat{a}_1^\dagger \to \cos\frac{Jt}{\hbar}\hat{a}_1^\dagger + i\sin\frac{Jt}{\hbar}\hat{a}_2^\dagger, \quad (4a)$$

$$\hat{a}_2^\dagger \to i\sin\frac{Jt}{\hbar}\hat{a}_1^\dagger + \cos\frac{Jt}{\hbar}\hat{a}_2^\dagger. \quad (4b)$$

Thus, $|\psi^o(t)\rangle = \frac{1}{\sqrt{N!}}(\cos(Jt/\hbar)\hat{a}_1^\dagger + i\sin(Jt/\hbar)\hat{a}_2^\dagger)^N|0\rangle$, where the superscript o represents the result of a non-interacting system. Extending t to the complex plane, we find that all zeros of $G(z)$ are located on the real axis with multiplicity N. When $z = t_k^o \equiv (k+1/2)T$, where k is an integer, the quantum state becomes $|0, N\rangle = \frac{1}{\sqrt{N!}}\hat{a}_2^{\dagger N}|0\rangle$, and $G(t_k^o) = 0$. One can view each identical boson as a spin-1/2. All spin-1/2s initially at the north pole of the Bloch sphere move to the south pole at the same times t_k^o, leading to a vanishing $G(z)$.

As shown in Fig. 1(c), a weak interaction satisfying $UN^2 \ll J$ has negligible effects at small times. A

given multiple zero with multiplicity N splits into N simple zeros, all of which are close to zeros of non-interacting systems. Indeed, $|\psi(t)\rangle$ is very similar to that of a non-interacting case, as shown in Fig. 2(a-d). For instance, at time $t = t^o \pm T/4$, $|\psi(t)\rangle$ is well represented by $\frac{1}{\sqrt{2^N N!}}(\hat{a}_1^\dagger \pm i\hat{a}_2^\dagger)^N|0\rangle$, corresponding to a binomial distribution when expanded by Fock states $|l\rangle \equiv |N/2+l, N/2-l\rangle$. To simplify notations, we consider even N here. See Appendix C for results of odd N. However, at large times, even a weak interaction has profound effects. As shown in Fig. 1(a), the separation between different zeros of $G(z)$ gets amplified greatly. Near t^*, these zeros deviate largely from those of non-interacting systems. Whereas such zeros have finite imaginary parts, they intrinsically affect physical observables in the real time axis, as shown later.

IV. DYNAMICALLY GENERATED ENTANGLED STATES.

We evaluate s-body correlation functions in the real time axis, $g_s = \langle\psi(t)|\,\hat{a}_1^{\dagger s}\hat{a}_2^s\,|\psi(t)\rangle, s \in \mathbb{Z}^+$. At $t = 0$, the Fock state has vanishing g_s for any s. As time goes on, g_s increases as a result of tunnelings between the two quantum states. When $U = 0$, the dynamics is fully captured by Rabi oscillations. When $U \neq 0$, Fig. 1(b) shows that one-body correlation function, $g_1(t)$, decays due to interaction induced decoherence. However, normalized two-body and N-body correlation functions, $\frac{4g_2(t)}{N(N-1)}$ and $\frac{2g_N(t)}{N!}$, reach their maxima around $t = t^*$. In the vicinity of t^*, both $|g_2|$ and $|g_N|$ oscillate with a period $T/2$. This indicates the rise of highly entangled states with multi-particle correlations. As shown in Fig. 2(e-h), the four states showing up alternatively near t^* are well captured by

$$
\begin{aligned}
&\tilde{t}_0 = kT, && |C_-\rangle = \frac{\hat{a}_1^{\dagger N} - i\hat{a}_2^{\dagger N}}{\sqrt{2N!}}|0\rangle,\\
&\tilde{t}_1 = kT + \frac{T}{4}, && |P_-\rangle = \sum_{n=0}^{N}\frac{i^{N-n} - i^{n+1}}{p_n}\hat{a}_1^{\dagger n}\hat{a}_2^{\dagger N-n}|0\rangle,\\
&\tilde{t}_2 = kT + \frac{2T}{4}, && |C_+\rangle = \frac{\hat{a}_1^{\dagger N} + i\hat{a}_2^{\dagger N}}{i^{1-N}\sqrt{2N!}}|0\rangle,\\
&\tilde{t}_3 = kT + \frac{3T}{4}, && |P_+\rangle = \sum_{n=0}^{N}\frac{i^{N-n} + i^{n+1}}{i^{1-N}p_n}\hat{a}_1^{\dagger n}\hat{a}_2^{\dagger N-n}|0\rangle,
\end{aligned}
\tag{5}
$$

where $\tilde{t} = t - t^*$ and $p_n = n!(N-n)!\sqrt{\frac{2^{N+1}}{N!}}$. $|C_\pm\rangle$ are NOON states with vanishing $g_{s<N}$ and $|g_N| = N!/2$. We have verified that any $g_{s<N}$ does vanish when NOON states arise. For clarity of the plots, $g_{2<s<N}$ are not shown in Fig. 1.

$|P_\pm\rangle$ are called pair condensates, since their one-body correction function g_1 vanishes, and their two-body correlation function g_2 is of the order of N^2. Correspondingly, their two-body reduced density matrix, $\langle a_i^{\dagger 2}a_j^2\rangle$, has only one macroscopic eigenvalue proportional to N^2. Therefore, $|P_\pm\rangle$ and $|C_\pm\rangle$ have distinct properties. Eq. (4), which can be regarded as a rotation of the quantization of axis, swaps $|P_\pm\rangle$ and $|C_\pm\rangle$. There are always two types of such different entangled states in any reference frames. As shown later, when studying $|G(t)|^2 = |\langle\psi(0)|\,e^{-\frac{i}{\hbar}\hat{H}t}\,|\psi(0)\rangle|^2$ that characterizes the quantum memory of the initial state, the chosen $|\psi(0)\rangle$ fixes the quantization axis such that $|P_\pm\rangle$ in Eq. (5) becomes orthogonal to $|\psi(0)\rangle$ when $N \to \infty$.

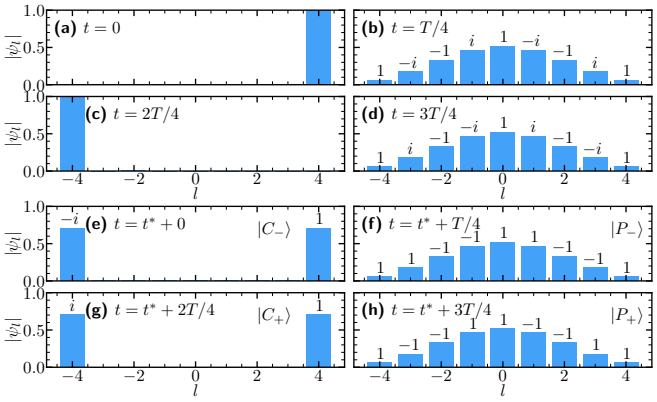

FIG. 2. (color online) (a-d) depicts the wave function expanded by Fock states $|\psi(t)\rangle = \sum\psi_l\left|\frac{N}{2}+l, \frac{N}{2}-l\right\rangle$ at four times $t = 0, T/4, 2T/4, 3T/4$. (e-h) are the results at four times near t^*. Numbers on top of bars represent relative phases of ψ_l. All parameters are identical to those in Fig. 1.

The energy spectrum in the limit $UN^2 \ll J$ (Appendix A), which is written as

$$E_n = An + Bn^2,\ n = 0, 1, .., N, \tag{6}$$

$$B = -\frac{U}{2},\quad A = \frac{UN}{2} + 2J,\quad r \equiv \frac{A}{B}. \tag{7}$$

For any initial state $|\psi(0)\rangle = \sum_{n=0}^N c_n|E_n\rangle$, the wave function at a later time is given by $|\psi(t)\rangle = \sum_{n=0}^N c_n e^{-\frac{i}{\hbar}E_n t}|E_n\rangle$. Tuning J and U, when $r = r_m$ is satisfied, where $r_m = 4m+2$ or $4m$, $m \in \mathbb{Z}$, $|C_\pm\rangle$ can be easily identified. If $r = 4m$, we obtain

$$|\Psi(t^*)\rangle = \sum_{n=0}^N c_n e^{-\frac{i}{\hbar}E_n t^*}|E_n\rangle = \sum_{n=0}^N c_n\frac{1-i(-1)^n}{\sqrt{2}}|E_n\rangle. \tag{8}$$

Because of the aforementioned symmetry of H in Eq. (2), the energy eigenstates have well defined parity,

$$\hat{P}|E_n\rangle = (-1)^n|E_n\rangle, \tag{9}$$

where $\hat{P}$ is the inversion operator, $\hat{P}|n_1, n_2\rangle = |n_2, n_1\rangle$ and $[\hat{H}, \hat{P}] = 0$. Using Eq. (8) and (9), we conclude that $|\psi(t^*)\rangle = (|\psi(0)\rangle - i\hat{P}|\psi(0)\rangle)/\sqrt{2}$. Whereas this result is valid for any initial state, the initial state we chose gives rise to $|C_-\rangle$ emerging at $t = t^*$. Meanwhile, interaction effects are negligible in a short time scale of a

few Ts. The time evolution in such time scale is well captured by Eq. (4) if we replace t by $t-t^*$. Applying such transformation to $|C_-\rangle$, it is straightforward to show that the other three states in Eq. (5) show up in corresponding times. If $r=4m+2$, the same discussions apply and the four states, $|C_+\rangle$, $|P_+\rangle$, $|C_-\rangle$ and $|P_-\rangle$, show up at times $\tilde{t}_0, \tilde{t}_1, \tilde{t}_2, \tilde{t}_3$ in Eq. (5). It is also worth mentioning that, for odd particle numbers, the pair condensates are described by another type of wave functions $\sim \sum_l \psi'_l \hat{a}_1^{\dagger 2l} \hat{a}_2^{\dagger N-2l}|0\rangle$ (Appendix C).

When $r \neq r_m$, Eq. (8) can not be satisfied. Nevertheless, the states near $t=t^*$ are well approximated by NOON states in the weakly interacting regime. We calculate the fidelity,

$$P(t) = \max(|\langle C_+|\psi(t)\rangle|^2, |\langle C_-|\psi(t)\rangle|^2). \tag{10}$$

Near t^*, we obtain (Appendix E)

$$P(t) \approx \sqrt{\frac{1}{1+\frac{N^2}{4}(\frac{\pi}{2}-\frac{U}{2\hbar}t)^2}} \times \sum_k \left| \exp\left(-\frac{1}{\frac{2}{N}+i(\frac{\pi}{2}-\frac{U}{2\hbar}t)} (\frac{k\pi}{2} - \frac{\pi N}{4} - \frac{Jt}{\hbar})^2 \right) \right|^2. \tag{11}$$

Near t^*, $P(t)$ consists of gaussian peaks centered at a series of discrete times with a separation $T/2$. Since the width of those peaks is about $\frac{\hbar}{\sqrt{N}J}$, only one peak contributes to $P(t)$ significantly at any t in the large N limit. $P(t)$ reaches its maximum at $t^{*\prime} = \frac{k_0\pi\hbar}{2J} - \frac{\pi N\hbar}{4J}$, and

$$\max[P(t)] = (1+(\frac{N\pi U d}{8J})^2)^{-1/2}, \tag{12}$$

where k_0 is the integer nearest to $\frac{2J}{U}+\frac{N}{2}$, $k_0 \equiv \mathrm{Int}(\frac{2J}{U}+\frac{N}{2})$, and $d \equiv |\frac{2J}{U}+\frac{N}{2}-k_0| \leqslant \frac{1}{2}$. When $r=r_m$, previous results are recovered because $\frac{2J}{U}+\frac{N}{2} = -\frac{r_m}{2}$ is an integer and $\max[P(t)]=1$. For generic $r \neq r_m$, the lower bound of $\max[P(t)]$ is written as $(1+(\frac{\pi NU}{16J})^2)^{-1/2}$. Thus, in the weakly interacting limit, NOON states well represent $|\psi(t^{*\prime})\rangle$. Away from $t=t^*$, we have numerically computed the overlaps between $|\psi(t)\rangle$ and the four states in Eq. (5), and such overlaps reach their maxima near t^* (Appendix D).

V. DQPT IN THE LARGE N LIMIT.

In a short time scale of a few Ts, the dynamics near t^* is well captured by Eq. (4) with the substitution $\tilde{t} = t - t^*$. Zeros of $G(z)$ are obtained analytically. For instance, when $r=4m$,

$$G(z) = \frac{1}{\sqrt{2}}((\cos\frac{J(z-t^*)}{\hbar})^N - i(i\sin\frac{J(z-t^*)}{\hbar})^N). \tag{13}$$

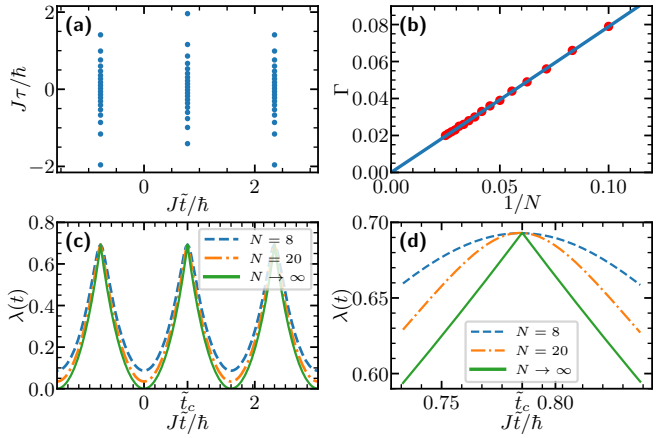

FIG. 3. (color online) (a) Zeros of $G(z)$ near t^* for $N=40$ particles ($\tilde{t} \equiv t-t^*$). (b) Distances between the real time axis and the nearest zeros around t^* as a function of $1/N$. The blue solid line is the analytical result from Eq. (14) and the red dots are numerical results. (c) The rate function $\lambda(t)$. (d) $\lambda(t)$ near $\tilde{t}_c$. $UN^2/J = 0.01$ has been used.

Fig. 3(a) shows that real parts of these zeros are given by $\mathrm{Re}\, z = t^* + (\frac{\pi}{4}+\frac{m}{2}\pi)\frac{\hbar}{J}, m \in \mathbb{Z}$, i.e., they are aligned in vertical lines in the complex plane. When N is odd, some zeros reside on the real axis (Appendix C). However, for a generic finite N, all zeros are away from the real axis. With increasing N, zeros become denser and gradually approach the real axis. The distance between the real axis and the nearest zero is bounded by

$$\Gamma = \frac{1}{2}\,\mathrm{arccosh}\,\frac{1}{|\cos\frac{\pi}{2N}|}. \tag{14}$$

In the large N limit, $\Gamma \approx \frac{\pi}{4N}$. Such scaling behavior is verified by numerical calculations, as shown in Fig. 3(b). When $N\to\infty$, straight lines formed by continuous zeros intersect with the real axis and lead to a vanishing $G(z)$ in the real axis. Correspondingly, $\lambda(t)$ becomes nonanalytic, signifying DQPTs. As shown in Fig. 3(c,d), near the transition point, $\lambda(t) = \ln 2 - 2\frac{J}{\hbar}|\tilde{t}-\tilde{t}_c|$ when $N\to\infty$, where $\tilde{t}_c = (\frac{\pi}{4}+\frac{m}{2}\pi)\frac{\hbar}{J}$. Comparing DQPT points and the times given in Eq. (5), we conclude that pair condensates, $|P_\pm\rangle$, reside at DQPT points and characterize the DQPT between two different types of NOON states, $|C_\pm\rangle$. This can also been seen from Fig. 1(e,f). Zeros of $G(z)$ near t^* are aligned in a vertical line, directly corresponding to maximized g_2.

VI. EFFECTS OF PERTURBATIONS.

Whereas essentially all parameters in Eq. (2) can be fine tuned, it is useful to consider effects of perturbations. We consider two types of important perturbations. (a) With increasing U, Eq. (6) includes high order terms $n^{s>2}$. (b) An energy mismatch $\Delta(n_1-n_2)$ breaks the inversion symmetry.

Consider (a), the lowest order contribution is a cubic term and we have $E_n = An + Bn^2 + Cn^3$, where $Cn^3 = -n^3U^2/(8J)$. The wave function is written as

$$|\Psi(t)\rangle = \sum_{n=0}^{n} c_n e^{-\frac{i}{\hbar}(An+Bn^2-\frac{U^2}{8J}n^3)t}, \tag{15}$$

where $c_n = (\frac{2}{\pi N})^{\frac{1}{4}} e^{-\frac{1}{N}(n-\frac{N}{2}-\frac{U}{16J}N^2)^2}$. If $\frac{U^2}{8J}n^3t^* \ll 1$ then the extra phase introduced by the cubic term is negligible within the time scale that is relevant to the emergent NOON states and DQPTs. Since c_n is a Gaussian with a width $\sqrt{N}$, which provides a natural cutoff of n in the sum in Eq. (15), we replace n in the above inequality by $\sqrt{N}$ and obtain $UN^{\frac{3}{2}} \ll J$. Thus, when $UN^2 \ll J$ is satisfied, all these corrections are negligible. Similar conclusions apply to $n^{s>2}$ caused by multi-body interactions (Appendix F).

For symmetry-breaking terms in (b), our calculation shows that a finite Δ suppresses g_N by a factor,

$$\frac{g_N}{g_N^0} = 1 - \left(\frac{\Delta^2 N}{2J^2} + \frac{U\Delta N(N-1)}{16J^2}\right), \tag{16}$$

where $g_N^0 = N!/2$ is the N-body correlation function of a NOON state. Thus, when

$$8\Delta^2 N + \Delta UN(N-1) \ll 16J^2 \tag{17}$$

all characteristic features of NOON states retain.

We compare Eq. (17) to the criterion for a stable NOON state at equilibrium [47], where a finite Δ strongly suppresses the superposition of $|N,0\rangle$ and $|0,N\rangle$, as a large N amplifies the energy penalty. Meanwhile, the effective tunneling between $|N,0\rangle$ and $|0,N\rangle$ is exponentially small, as it requires N steps of single-particle tunneling to couple them. $\Delta N \ll Je^{-N}$ is then required, i.e., an exponentially small Δ with increasing N. Here, such a constraint does not apply in non-equilibrium dynamics. Eq. (17) shows that, with increasing N, Δ only needs to be suppressed as a power law. The dynamically generated NOON states are much more stable than their counterparts at equilibrium. Thus, our results suggest a new route to access NOON states that can be potentially used in precision measurements.

VII. EXPERIMENTAL REALIZATIONS AND CONCLUSIONS

Whereas our results apply to generic atomic interferometers with any particle number, we comment on possible sceneries directly related to current experiments. Optical tweezers has recently been used to create an atomic Hong-Ou-Mandel interferometer [13]. Each single tweezer corresponds to a quantum state in Eq. (2), and both interaction U and tunneling J can be tuned. Trapping multiple atoms is also possible [48, 49]. Using realistic experimental parameters $J/2\pi = 262(4)$Hz in [13], when $U/J = 0.022$ and $N = 8$, NOON states and DQPTs emerge around a critical time about 86ms (Appendix G). Beside optical tweezers, other systems ranging from double-well optical lattices to mesoscopic traps [50–53], in which the total particle number can be controlled precisely, are also suitable for testing our theoretical results. In addition, H in Eq. (2) can be mapped to a spin-1/2 model with all-to-all interactions [54], which offers another realization of our schemes in spin systems.

We have studied DQPTs in interacting atomic interferometers and shown that dynamically generated entangled states have deep connections with zeros of Loschmidt echo in the complex plane. DQPTs provide us with a new angle to understand non-equilibrium dynamics. We hope that our work will stimulate more interests of using interacting interferometers to explore DQPTs and to produce novel entangled quantum states.

ACKNOWLEDGMENTS

This work is supported by startup funds from Purdue University. C. Lyu also acknowledges the support of F. N. Andrews Fellowship from Purdue University.

Appendix A: Eigenstates and energy spectrum of the Hamiltonian

We consider the Hamiltonian $\hat{H} = -J(\hat{a}_1^\dagger \hat{a}_2 + \hat{a}_2^\dagger \hat{a}_1) + \frac{U}{2}(\hat{n}_1+\hat{n}_2)^2 + \frac{U}{4}(\hat{n}_1-\hat{n}_2)^2 + \Delta(\hat{n}_1-\hat{n}_2)$. When $U = \Delta = 0$, the eigenenergies E_n^0 and eigenstates $|E_n^0\rangle$ are

$$E_n^0 = 2J(n - \frac{N}{2}), \tag{A1}$$

$$|E_n^0\rangle = \frac{1}{\sqrt{n!(N-n)!}}(\frac{\hat{a}_1^\dagger + \hat{a}_2^\dagger}{\sqrt{2}})^{N-n}(\frac{\hat{a}_1^\dagger - \hat{a}_2^\dagger}{\sqrt{2}})^n |0\rangle . \tag{A2}$$

When $U, \Delta \ll J$, the first and second order corrections to the eigenenergies are

$$E_n^1 = \frac{U}{4}(2nN - 2n^2 + N), \tag{A3}$$

$$E_n^2 = \frac{U^2}{32J}(2n-N)(N-1+2Nn-2n^2) + \frac{\Delta^2}{2J}(2n-N). \tag{A4}$$

The eigenstates are

$$\begin{aligned}|E_n\rangle = |E_n^0\rangle &- \frac{\Delta}{2J}\sqrt{(n+1)(N-n)}\,|E_{n+1}^0\rangle \\ &+ \frac{\Delta}{2J}\sqrt{n(N-n+1)}\,|E_{n-1}^0\rangle + O(\Delta^3) \\ &- \frac{U}{4}\frac{\sqrt{(N-n)(N-n-1)(n+1)(n+2)}}{4J}\,|E_{n+2}^0\rangle \\ &+ \frac{U}{4}\frac{\sqrt{(n-1)n(N-n+1)(N-n+2)}}{4J}\,|E_{n-2}^0\rangle .\end{aligned} \tag{A5}$$

Appendix B: Attractive interactions

As discussed in the main text, when $U>0$, $t^*=\frac{\pi\hbar}{U}$, and $r_m=4m$, $|C_-\rangle$, $|P_-\rangle$, $|C_+\rangle$, and $|P_+\rangle$ show up in order starting from t^*. In contrast, $r_m=4m+2$, $|C_+\rangle$, $|P_+\rangle$, $|C_-\rangle$, and $|P_-\rangle$ show up in order starting from t^*.

Here we discuss $U<0$ and $t^*=\frac{\pi\hbar}{|U|}$. (1) $r_m=4m$, $|C_+\rangle$, $|P_+\rangle$, $|C_-\rangle$, and $|P_-\rangle$ show up in order starting from t^*, and $G(z)=\frac{1}{\sqrt{2}}((\cos J(z-t^*)/\hbar)^N+i(i\sin J(z-t^*)/\hbar)^N)$. (2) $r_m=4m+2$, $|C_-\rangle$, $|P_-\rangle$, $|C_+\rangle$, and $|P_+\rangle$ show up in order starting from t^*, and $G(z)=\frac{1}{\sqrt{2}}((\cos J(z-t^*)/\hbar)^N-i(i\sin J(z-t^*)/\hbar)^N)$.

If r_m is not an even integer, Eq. (11) can be generalized to

$$P(t)\approx\sqrt{\frac{1}{1+\frac{N^2}{4}(\frac{\pi}{2}-\frac{|U|}{2\hbar}t)^2}}\times \sum_k\left|\exp\left(-\frac{1}{\frac{2}{N}+i\frac{U}{|U|}(\frac{\pi}{2}-\frac{|U|}{2\hbar}t)}(\frac{k\pi}{2}-\frac{\pi N}{4}-\frac{Jt}{\hbar})^2\right)\right|^2. \tag{B1}$$

Appendix C: Results for odd number of particles

The zeros of $G(z)=\frac{1}{\sqrt{2}}((\cos J(z-t^*)/\hbar)^N\pm i(i\sin J(z-t^*)/\hbar)^N)$ are written as

$$\mathrm{Re}\,\frac{J(z-t^*)}{\hbar}=\frac{\pi}{4}+\frac{l}{2}\pi, l\in\mathbb{Z}, \tag{C1}$$

$$\mathrm{Im}\,\frac{J(z-t^*)}{\hbar}=\frac{1}{2}\,\mathrm{arccosh}\,\frac{1}{|\cos\pi(\frac{1+2k\mp1/2}{N}-\frac{1}{2})|} \times\mathrm{sgn}\sin\pi(\frac{1+2k\mp1/2}{N}-\frac{1}{2}),\quad k=1,2,...,N. \tag{C2}$$

For a finite even N, zeros have finite imaginary parts. For a finite odd N, some zeros reside on the real time axis, as shown in Fig. 4.

In the large N limit: (1) If N is even, $\lim_{N\to\infty}\lambda(t)=-2\ln[\max(|\cos J\tilde{t}/\hbar|,|\sin J\tilde{t}/\hbar|)]$, which has been analyzed in the main text. (2) If N is odd, $\lambda_\pm(t)=-\frac{1}{N}\ln\left(\frac{1}{2}|\cos^N J\tilde{t}/\hbar\pm\sin^N J\tilde{t}/\hbar|^2\right)$. The sign $\pm$ is determined by the sign before i in $G(t)$ and whether $N=4p+1$ or $4p+3$, $p\in\mathbb{Z}$. $\lambda_\pm(t)$ is nonanalytic at $\tilde{t}_c=\frac{\hbar}{J}(\frac{\pi}{4}+k\frac{\pi}{2}), k\in\mathbb{Z}$, when $N\to\infty$. Especially, $\lim_{N\to\infty}\lambda_-(t)=-2\ln[\max(|\cos J\tilde{t}/\hbar|,|\sin J\tilde{t}/\hbar|)]$ except at $\tilde{t}_{c1}=\frac{\hbar}{J}(\frac{\pi}{4}+k\pi), k\in\mathbb{Z}$. As shown in Fig. 4(d), $\lambda_-(t)$ diverges at $\tilde{t}_{c1}$ for any finite odd N. Similar conclusions apply to $\lambda_+(t)$.

The emerged pair condensates near t^* for odd N are also different from those for even N, Using Eq. (4), for $N=2m+1, m\in\mathbb{Z}$, we obtain,

$$\begin{aligned}|P_-\rangle&=\sum_{n=0}^{N}\frac{i^{N-n}-i^{n+1}}{p_n}\hat{a}_1^{\dagger n}\hat{a}_2^{\dagger N-n}|0\rangle\\&=\sum_{n=0}^{N}\frac{i^{n+1}((-1)^{m+n}-1)}{p_n}\hat{a}_1^{\dagger n}\hat{a}_2^{\dagger N-n}|0\rangle,\end{aligned} \tag{C3}$$

$$\begin{aligned}|P_+\rangle&=\sum_{n=0}^{N}\frac{i^{N-n}+i^{n+1}}{p_n}\hat{a}_1^{\dagger n}\hat{a}_2^{\dagger N-n}|0\rangle\\&=\sum_{n=0}^{N}\frac{i^{n+1}((-1)^{m+n}+1)}{p_n}\hat{a}_1^{\dagger n}\hat{a}_2^{\dagger N-n}|0\rangle.\end{aligned} \tag{C4}$$

Thus, some Fock states are suppressed by the factor $(-1)^{m+n}-1$. For instance when $N=7$, $|P_-\rangle$ only contains $|0,7\rangle,|2,5\rangle,|4,3\rangle,|6,1\rangle$. Apparently both one-body correction g_1 and $G(t)=\langle7,0|P_-\rangle$ vanishes.

Appendix D: Overlaps between $|\psi(t)\rangle$ and $|C_\pm\rangle$, $|P_\pm\rangle$.

Away from t^*, there is no simple analytical expression for the overlap between $|\psi(t)\rangle$ and the NOON states or pair condensates. We thus evaluate such overlaps numerically, as shown in Fig. 5. Near $t^*=\frac{\pi\hbar}{U}$, the four states defined in Eq. (4) show up alternatively. The overlaps reach maxima near t^*.

Appendix E: Detailed analyses of perturbations

When $\Delta=0$, the initial state $|N,0\rangle$ can be expanded by energy eigenstates and the coefficients c_n are

$$\begin{aligned}|c_n|^2&=|\langle E_n|N,0\rangle|^2\\&=|\frac{1}{2^{N/2}}\sqrt{\frac{N!}{n!(N-n)!}}(1-(N-2n)\frac{U(N-1)}{16J})|^2\\&\approx\sqrt{\frac{2}{\pi N}}e^{-\frac{2}{N}((n-\frac{N}{2})-\frac{UN(N-1)}{16J})^2}.\end{aligned} \tag{E1}$$

Assuming $E_n=Cn^3+Bn^2+An$ and $B<0$, the overlap between $|\psi_t\rangle$ and the NOON state $(|N,0\rangle+i|0,N\rangle)/\sqrt{2}$ is

$$\begin{aligned}\langle C_+|\psi(t)\rangle&=\sum_{n=0}^{N}|c_n|^2e^{-i(\frac{\pi}{2}n^2+n\pi)}e^{-\frac{i}{\hbar}E_nt}\\&=\sum_m\sqrt{\frac{2}{\pi N}}e^{-\frac{2}{N}m^2-\frac{iCt}{\hbar}m^3-i(\frac{\pi}{2}-H_2t)m^2+i(G_1-\pi-H_1t)m},\end{aligned} \tag{E2}$$

where $m = n - \frac{N}{2} + \frac{UN^2}{16J}$ and

$$H_2 = \frac{|B|}{\hbar} - \frac{3CN^2U}{16\hbar J} - \frac{3CN}{2\hbar}, \tag{E3}$$

$$H_1 = \frac{A}{\hbar} - \frac{|B|N^2U}{8\hbar J} - \frac{|B|N}{\hbar} + \frac{3CN^4U^2}{256\hbar J^2} + \frac{3CN^3U}{16\hbar J} + \frac{3CN^2}{4\hbar}, \tag{E4}$$

$$G_1 = -\frac{\pi N^2 U}{16J} - \frac{\pi N}{2}. \tag{E5}$$

What is required is that the phase contributed by the cubic term is negligible when $t \sim \frac{\pi\hbar}{U}$. Since the width of the gaussian factor is $\sqrt{N}$, we require

$$|\frac{Ct}{\hbar}m^3| = |\frac{U^2}{8J}\frac{\pi}{U}N^{3/2}| \ll 1 \Rightarrow |\frac{UN^{3/2}}{J}| \ll 1, \tag{E6}$$

where we have used the energy spectrum obtained from second order perturbation. The cubic term is then dropped and we employ Poisson summation formula to obtain

$$\langle C_+|\psi(t)\rangle = \sum_k \sqrt{\frac{1}{1+i\frac{N}{2}(G_2 - H_2 t)}}\times \exp\left(-\frac{1}{\frac{2}{N}+i(G_2-H_2t)}(\frac{(2k-1)\pi + G_1}{H_1} - t)^2\frac{H_1^2}{4}\right). \tag{E7}$$

Similarly, we obtain

$$\langle C_-|\psi(t)\rangle = \sum_k \sqrt{\frac{1}{1+i\frac{N}{2}(G_2 - H_2 t)}}\times \exp\left(-\frac{1}{\frac{2}{N}+i(G_2-H_2t)}(\frac{(2k)\pi + G_1}{H_1} - t)^2\frac{H_1^2}{4}\right). \tag{E8}$$

When Eq. (E6) is satisfied, $H_2 \approx \frac{|B|}{\hbar} \approx \frac{U}{2\hbar}$, $H_1 \approx \frac{A}{\hbar} \approx \frac{2J}{\hbar}$, and $G_1 \approx -\frac{\pi N}{2}$. We define the probability of finding a NOON state as $P(t) = \max(|\langle C_+|\psi(t)\rangle|^2, |\langle C_-|\psi(t)\rangle|^2)$. Near $t = \frac{G_2}{H_2}$, $P(t)$ can be written as

$$P(t) \approx \sqrt{\frac{1}{1+\frac{N^2}{4}(\frac{\pi}{2}-\frac{U}{2\hbar}t)^2}}\times \sum_k \left|\exp\left(-\frac{1}{\frac{2}{N}+i(\frac{\pi}{2}-\frac{U}{2\hbar}t)}(\frac{k\pi\hbar}{2J} - \frac{\pi N\hbar}{4J} - t)^2\frac{J^2}{\hbar^2}\right)\right|^2. \tag{E9}$$

$P(t)$ consists of multiple gaussian functions whose peaks are located at $t = \frac{k\pi\hbar}{2J} - \frac{\pi N\hbar}{4J}, k \in \mathbb{Z}$, and their separation is $\frac{\pi\hbar}{2J}$. There is also a factor $(1 + \frac{N^2}{4}(\frac{\pi}{2} - \frac{U}{2\hbar}t)^2)^{-1/2}$, which suppresses peak heights. If the parameters are fine tuned such that an integer k_0 satisfies $\frac{\pi}{2} - \frac{U}{2\hbar}(\frac{k_0\pi\hbar}{2J} - \frac{\pi N\hbar}{4J}) = 0$, then $P(t) = 1$ at $t = \frac{k_0\pi\hbar}{2J} - \frac{\pi N\hbar}{4J}$. We thus obtain a perfect NOON state. Without fine tuning the parameters, we consider $t = \frac{\pi\hbar}{U}$ that lies in the middle of two peaks. The two peaks get a suppression of $(1 + (\frac{\pi NU}{16J})^2)^{-1/2}$. Again, because of Eq. (E6), this factor is negligible when N is large.

If the energy mismatch Δ is finite, we separate the eigenstates into two parts according to their spatial parity,

$$|E_n\rangle = \alpha_n |E_n\rangle_s + \beta_n |E_n\rangle_a, \tag{E10}$$

$$\hat{P}|E_m\rangle = \alpha_n(-1)^n |E_n\rangle_s + \beta_n(-1)^{n+1}|E_n\rangle_a. \tag{E11}$$

The time evolution of the wave function is written as $|N,0\rangle \to |\psi_t\rangle = \sum_{n=0}^N c_n\alpha_n e^{-iE_nt}|E_n\rangle_s + c_n\beta_n e^{-iE_nt}|E_n\rangle_a$. From Eq. (A4), we see that, up to the second order of Δ, the quadratic term in E_n remains unchanged. Thus, when $t^* = \frac{\pi\hbar}{U}$, $e^{-iE_nt^*} = \frac{1+i(-1)^n}{\sqrt{2}}$ is satisfied, and we obtain

$$\begin{aligned}|\psi(t^*)\rangle &= \sum_{n=0}^N \alpha_n c_n \frac{1+i(-1)^n}{\sqrt{2}}|E_n\rangle_s \\ &\quad + \beta_n c_n \frac{1+i(-1)^n}{\sqrt{2}}|E_n\rangle_a \\ &= |cat\rangle + |err\rangle,\end{aligned} \tag{E12}$$

where $|err\rangle = \sum_{n=0}^N i\sqrt{2}(-1)^n c_n\beta_n|E_n\rangle_a$ is the correction to the NOON state at t^*, and

$$\begin{aligned}g_N &= \langle\psi_{t^*}|\hat{a}_1^{\dagger N}\hat{a}_2^N|\psi_{t^*}\rangle \\ &= g_N^0 + \frac{N!}{\sqrt{2}}\langle 0,N|err\rangle + i\frac{N!}{\sqrt{2}}\langle err|N,0\rangle \\ &\quad + \langle err|\hat{a}_1^{\dagger N}\hat{a}_2^N|err\rangle\end{aligned} \tag{E13}$$

Using Eq. (A5), we obtain

$$\beta_n|E_n\rangle_a = -\frac{\Delta}{2J}\sqrt{(n+1)(N-n)}|E_{n+1}^0\rangle + \frac{\Delta}{2J}\sqrt{n(N-n+1)}|E_{n-1}^0\rangle + O(\Delta^3). \tag{E14}$$

Up to the first order of U and Δ,

$$|err\rangle^{(1)} = \frac{\Delta}{2J}\sum_{n=0}^N i\sqrt{2}\frac{(-1)^{n+1}}{2^{N/2}}\sqrt{\frac{N!}{n!(N-n)!}}(N-2n)|E_n^0\rangle. \tag{E15}$$

It is straightforward to verify that $\langle 0,N|err\rangle^{(1)}$, $\langle err|^{(1)}|N,0\rangle$ and $\hat{a}_1^{\dagger N}\hat{a}_2^N|err\rangle^{(1)}$ vanish.

Up to the second order of U and Δ,

$$|err\rangle^{(2)} = \frac{\Delta}{2J}(\frac{\Delta}{2J} + \frac{U(N-1)}{16J})\times \sum_{n=0}^N i\sqrt{2}\frac{(-1)^{n+1}}{2^{N/2}}\sqrt{\frac{N!}{n!(N-n)!}}(N-2n)^2|E_n^0\rangle, \tag{E16}$$

So,

$$\langle 0,N|err\rangle^{(2)} = -i\sqrt{2}\frac{\Delta}{2J}(\frac{\Delta}{2J}+\frac{U(N-1)}{16J})\frac{N!}{(N-1)!}, \tag{E17}$$

$$\langle err|^{(2)}|N,0\rangle = 0. \tag{E18}$$

Therefore,

$$\begin{aligned} g_N =& \langle\psi(t^*)|\,\hat{a}_1^{\dagger N}\hat{a}_2^N\,|\psi(t^*)\rangle \\ =& i\frac{N!}{2} - i(\frac{\Delta}{2J}(\frac{\Delta}{2J}+\frac{U(N-1)}{16J}))\frac{N!^2}{(N-1)!} \\ =& g_N^0(1-2N(\frac{\Delta}{2J}(\frac{\Delta}{2J}+\frac{U(N-1)}{16J}))). \end{aligned} \tag{E19}$$

Appendix F: Multi-body interactions

Interaction induced inter-band couplings may lead to virtual transitions of particles from the lowest energy band to higher bands [41]. When the band gap is small compared to the interaction strength, there exist effective multi-body interactions. As for the three body interaction, $U_3(n_1^3+n_2^3)$, it can be rewritten as $U_3(n_1+n_2)^3 - 3U_3n_1n_2(n_1+n_2)$. Because of the conservation of the total particle number, the first term is not relevant to the dynamics. The second term turns the two-body interaction, U, discussed in the main text into $U \to U+3U_3N$, and does not change any qualitative results.

Other multi-body interactions do not change our results neither, provided that they respect the inversion symmetry. As discussed in the main text, NOON states emergent in the dynamics are protected by the inversion symmetry. Any multi-body interactions, $U_{s>2}(n_1^s+n_2^s)$, still respect this symmetry. Thus, the only effect that they have on the dynamics is to add corrections, $n^{s>2}$, to the energy spectrum in Eq. (5) of the main text. Any such small corrections would not affect the qualitative results of the dynamics in short times, similar to the discussions on Eq. (14) of the main text.

Appendix G: Correlation functions and zeros of $G(z)$ in optical tweezers

Two coupled optical tweezers have been used to create an atomic Hong-Ou-Mandel interferometer [12, 13]. Starting from an initial state, $|2,0\rangle$, i.e., two bosons occupy the same optical tweezer, the time evolution of the correlation functions can be calculated analytically,

$$\begin{aligned} g_1 =& -\frac{2U}{\sqrt{16J^2+U^2}}\alpha\beta\sin^2\frac{\sqrt{16J^2+U^2}t}{2\hbar} \\ &+ i2\alpha\beta\sin\frac{\sqrt{16J^2+U^2}t}{2\hbar}\cos\frac{Ut}{2\hbar} \end{aligned} \tag{G1}$$

$$\begin{aligned} g_2 =& \frac{\alpha^4+\beta^4-1}{2} + \alpha^2\beta^2\cos\frac{\sqrt{16J^2+U^2}t}{\hbar} \\ &+i\left(\sin\frac{Ut}{2\hbar}\cos\frac{\sqrt{16J^2+U^2}t}{2\hbar}\right. \\ &\left.-\frac{U}{\sqrt{16J^2+U^2}}\cos\frac{Ut}{2\hbar}\sin\frac{\sqrt{16J^2+U^2}t}{2\hbar}\right), \end{aligned} \tag{G2}$$

where $\alpha = \frac{1}{\sqrt{2}}\sqrt{1-\frac{U}{\sqrt{16J^2+U^2}}}, \beta = \frac{1}{\sqrt{2}}\sqrt{1+\frac{U}{\sqrt{16J^2+U^2}}}$. If the parameters are fine tuned such that $\frac{\sqrt{16J^2+U^2}}{U} = 2k, k\in\mathbb{Z}$, at $t^* = \frac{\pi\hbar}{U}$, we obtain, $g_1 = 0, g_2 = i(-1)^k$, and a small NOON state $\frac{|2,0\rangle+i(-1)^k|0,2\rangle}{\sqrt{2}}$. Using realistic experimental parameters in Ref. [13],

$J/2\pi = 262(4)$Hz and $U/J = 0.22(2)$, the correlation functions and the zeros of $G(z)$ are shown in Fig. 6. When $U \ll J$, $\frac{\sqrt{16J^2+U^2}}{U} = 2k$ corresponds to $r = r_m$ in the main text. Without fine tuning experimental parameters, there are corrections to the small NOON state at t^*, similar to the results discussed in the main text. It is worth mentioning that, starting from $|1,1\rangle$, the current experiment has shown that a small NOON state can be produced in a Hong-Ou-Mandel interferometer. However, this is only true when interactions are ignored. We have verified that, in the presence of interactions, $|1,1\rangle$ cannot produce a small NOON state. Instead, $|2,0\rangle$ should be used, as shown by the previous discussions.

It is possible that optical tweezers could trap multiple particles. For 8 particles, $UN^2 \ll J$ is no longer satisfied if $U/J = 0.22(2)$. Nevertheless, qualitative results remain unchanged. As shown in Fig. 7, g_8 is maximized near t^* while other correlation functions are suppressed. With U/J decreased down to 0.022, all results in the main text are recovered and the predicted NOON states and DQPTs can be observed around $t = 86$ms.

[1] J. B. Fixler, G. T. Foster, J. M. McGuirk, and M. A. Kasevich, Atom interferometer measurement of the newtonian constant of gravity, Science **315**, 74 (2007).

[2] S. Fray, C. A. Diez, T. W. Hänsch, and M. Weitz, Atomic interferometer with amplitude gratings of light and its applications to atom based tests of the equivalence principle, Phys. Rev. Lett. **93**, 240404 (2004).

[3] P. Cladé, E. de Mirandes, M. Cadoret, S. Guellati-Khélifa, C. Schwob, F. m. c. Nez, L. Julien, and F. m. c. Biraben, Determination of the fine structure constant based on bloch oscillations of ultracold atoms in a vertical optical lattice, Phys. Rev. Lett. **96**, 033001 (2006).

[4] P. W. Graham, J. M. Hogan, M. A. Kasevich, and S. Rajendran, New method for gravitational wave detection with atomic sensors, Phys. Rev. Lett. **110**, 171102 (2013).

[5] S. Dimopoulos, P. W. Graham, J. M. Hogan, M. A. Kasevich, and S. Rajendran, Atomic gravitational wave interferometric sensor, Phys. Rev. D **78**, 122002 (2008).

[6] J. Lawall and M. Prentiss, Demonstration of a novel atomic beam splitter, Phys. Rev. Lett. **72**, 993 (1994).

[7] S. Glasgow, P. Meystre, M. Wilkens, and E. M. Wright, Theory of an atomic beam splitter based on velocity-tuned resonances, Phys. Rev. A **43**, 2455 (1991).

[8] T. Pfau, C. Kurtsiefer, C. S. Adams, M. Sigel, and J. Mlynek, Magneto-optical beam splitter for atoms, Phys. Rev. Lett. **71**, 3427 (1993).

[9] O. Houde, D. Kadio, and L. Pruvost, Cold atom beam splitter realized with two crossing dipole guides, Phys. Rev. Lett. **85**, 5543 (2000).

[10] R. Grimm, J. Söding, and Y. B. Ovchinnikov, Coherent beam splitter for atoms based on a bichromatic standing light wave, Opt. Lett. **19**, 658 (1994).

[11] C. K. Hong, Z. Y. Ou, and L. Mandel, Measurement of subpicosecond time intervals between two photons by interference, Phys. Rev. Lett. **59**, 2044 (1987).

[12] A. M. Kaufman, B. J. Lester, and C. A. Regal, Cooling a single atom in an optical tweezer to its quantum ground state, Phys. Rev. X **2**, 041014 (2012).

[13] A. M. Kaufman, B. J. Lester, C. M. Reynolds, M. L. Wall, M. Foss-Feig, K. R. A. Hazzard, A. M. Rey, and C. A. Regal, Two-particle quantum interference in tunnel-coupled optical tweezers, Science **345**, 306 (2014).

[14] R. Lopes, A. Imanaliev, A. Aspect, M. Cheneau, D. Boiron, and C. I. Westbrook, Atomic hong-ou-mandel experiment, Nature **520**, 66 (2015).

[15] A. Buchleitner and A. R. Kolovsky, Interaction-induced decoherence of atomic bloch oscillations, Phys. Rev. Lett. **91**, 253002 (2003).

[16] J. T. Chalker, Y. Gefen, and M. Y. Veillette, Decoherence and interactions in an electronic mach-zehnder interferometer, Phys. Rev. B **76**, 085320 (2007).

[17] A. O. Jamison, J. N. Kutz, and S. Gupta, Atomic interactions in precision interferometry using bose-einstein condensates, Phys. Rev. A **84**, 043643 (2011).

[18] B. Juliá-Díaz, T. Zibold, M. K. Oberthaler, M. Melé-Messeguer, J. Martorell, and A. Polls, Dynamic generation of spin-squeezed states in bosonic josephson junctions, Phys. Rev. A **86**, 023615 (2012).

[19] M. Heyl, A. Polkovnikov, and S. Kehrein, Dynamical quantum phase transitions in the transverse-field ising model, Phys. Rev. Lett. **110**, 135704 (2013).

[20] M. Heyl and J. C. Budich, Dynamical topological quantum phase transitions for mixed states, Phys. Rev. B **96**, 180304(R) (2017).

[21] A. A. Zvyagin, Dynamical quantum phase transitions (review article), Low Temperature Physics **42**, 971 (2016).

[22] M. Heyl, Dynamical quantum phase transitions: a review, Reports on Progress in Physics **81**, 054001 (2018).

[23] C. N. Yang and T. D. Lee, Statistical theory of equations of state and phase transitions. i. theory of condensation, Phys. Rev. **87**, 404 (1952).

[24] M. E. Fisher, Yang-lee edge singularity and ϕ^3 field theory, Phys. Rev. Lett. **40**, 1610 (1978).

[25] M. Heyl, Dynamical quantum phase transitions in systems with broken-symmetry phases, Phys. Rev. Lett. **113**, 205701 (2014).

[26] P. Jurcevic, H. Shen, P. Hauke, C. Maier, T. Brydges, C. Hempel, B. P. Lanyon, M. Heyl, R. Blatt, and C. F. Roos, Direct observation of dynamical quantum phase transitions in an interacting many-body system, Phys. Rev. Lett. **119**, 080501 (2017).

[27] S. Smale, P. He, B. A. Olsen, K. G. Jackson, H. Sharum, S. Trotzky, J. Marino, A. M. Rey, and J. H. Thywissen, Observation of a transition between dynamical phases in a quantum degenerate fermi gas, Science Advances **5**, eaax1568 (2019).

[28] S. Sharma, U. Divakaran, A. Polkovnikov, and A. Dutta, Slow quenches in a quantum ising chain: Dynamical phase transitions and topology, Phys. Rev. B **93**, 144306 (2016).

[29] U. Bhattacharya, S. Bandyopadhyay, and A. Dutta, Mixed state dynamical quantum phase transitions, Phys. Rev. B **96**, 180303(R) (2017).

[30] L. Piroli, B. Pozsgay, and E. Vernier, Non-analytic behavior of the loschmidt echo in xxz spin chains: Exact results, Nuclear Physics B **933**, 454 (2018).

[31] P. Nozières and D. Saint James, Particle vs. pair condensation in attractive bose liquids, J. Phys. France **43**, 1133 (1982).

[32] U. R. Fischer and B. Xiong, Robustness of fragmented condensate many-body states for continuous distribution amplitudes in fock space, Phys. Rev. A **88**, 053602 (2013).

[33] K.-J. Chen, H. K. Lau, H. M. Chan, D. Wang, and Q. Zhou, Unfolding multi-particle quantum correlations hidden in decoherence, arXiv:1711.04105 (2017).

[34] M. Heyl, Scaling and universality at dynamical quantum phase transitions, Phys. Rev. Lett. **115**, 140602 (2015).

[35] A. Kosior and K. Sacha, Dynamical quantum phase transitions in discrete time crystals, Phys. Rev. A **97**, 053621 (2018).

[36] C. Karrasch and D. Schuricht, Dynamical quantum phase transitions in the quantum potts chain, Phys. Rev. B **95**, 075143 (2017).

[37] V. Giovannetti, S. Lloyd, and L. Maccone, Quantum-enhanced measurements: Beating the standard quantum limit, Science **306**, 1330 (2004).

[38] V. Giovannetti, S. Lloyd, and L. Maccone, Quantum metrology, Phys. Rev. Lett. **96**, 010401 (2006).

[39] V. Giovannetti, S. Lloyd, and L. Maccone, Advances in quantum metrology, Nature Photonics **5**, 222 (2011).

[40] D. Leibfried, M. D. Barrett, T. Schaetz, J. Britton, J. Chiaverini, W. M. Itano, J. D. Jost, C. Langer, and D. J. Wineland, Toward heisenberg-limited spectroscopy with multiparticle entangled states, Science **304**, 1476 (2004).

[41] S. Will, T. Best, U. Schneider, L. Hackermüller, D.-S. Lühmann, and I. Bloch, Time-resolved observation of coherent multi-body interactions in quantum phase revivals, Nature **465**, 197 (2010).

[42] G. J. Milburn, J. Corney, E. M. Wright, and D. F. Walls, Quantum dynamics of an atomic bose-einstein condensate in a double-well potential, Phys. Rev. A **55**, 4318 (1997).

[43] T.-L. Ho and C. V. Ciobanu, The schrödinger cat family in attractive bose gases, Journal of Low Temperature Physics **135**, 257 (2004).

[44] M. Albiez, R. Gati, J. Fölling, S. Hunsmann, M. Cristiani, and M. K. Oberthaler, Direct observation of tunneling and nonlinear self-trapping in a single bosonic joseph-

son junction, Phys. Rev. Lett. **95**, 010402 (2005).
[45] A. N. Salgueiro, A. de Toledo Piza, G. B. Lemos, R. Drumond, M. C. Nemes, and M. Weidemüller, Quantum dynamics of bosons in a double-well potential: Josephson oscillations, self-trapping and ultralong tunneling times, The European Physical Journal D **44**, 537 (2007).
[46] T. Zibold, E. Nicklas, C. Gross, and M. K. Oberthaler, Classical bifurcation at the transition from rabi to josephson dynamics, Phys. Rev. Lett. **105**, 204101 (2010).
[47] A. Micheli, D. Jaksch, J. I. Cirac, and P. Zoller, Many-particle entanglement in two-component bose-einstein condensates, Phys. Rev. A **67**, 013607 (2003).
[48] M. Li and J. Arlt, Trapping multiple particles in single optical tweezers, Optics Communications **281**, 135 (2008).
[49] C. A. Regal, (private communication).
[50] J. Sebby-Strabley, M. Anderlini, P. S. Jessen, and J. V. Porto, Lattice of double wells for manipulating pairs of cold atoms, Phys. Rev. A **73**, 033605 (2006).
[51] Y. Shin, M. Saba, T. A. Pasquini, W. Ketterle, D. E. Pritchard, and A. E. Leanhardt, Atom interferometry with bose-einstein condensates in a double-well potential, Phys. Rev. Lett. **92**, 050405 (2004).
[52] T. Schumm, S. Hofferberth, L. M. Andersson, S. Wildermuth, S. Groth, I. Bar-Joseph, J. Schmiedmayer, and P. Krüger, Matter-wave interferometry in a double well on an atom chip, Nature Physics **1**, 57 (2005).
[53] R. Islam, R. Ma, P. M. Preiss, M. Eric Tai, A. Lukin, M. Rispoli, and M. Greiner, Measuring entanglement entropy in a quantum many-body system, Nature **528**, 77 (2015).
[54] A. Russomanno, F. Iemini, M. Dalmonte, and R. Fazio, Floquet time crystal in the lipkin-meshkov-glick model, Phys. Rev. B **95**, 214307 (2017).

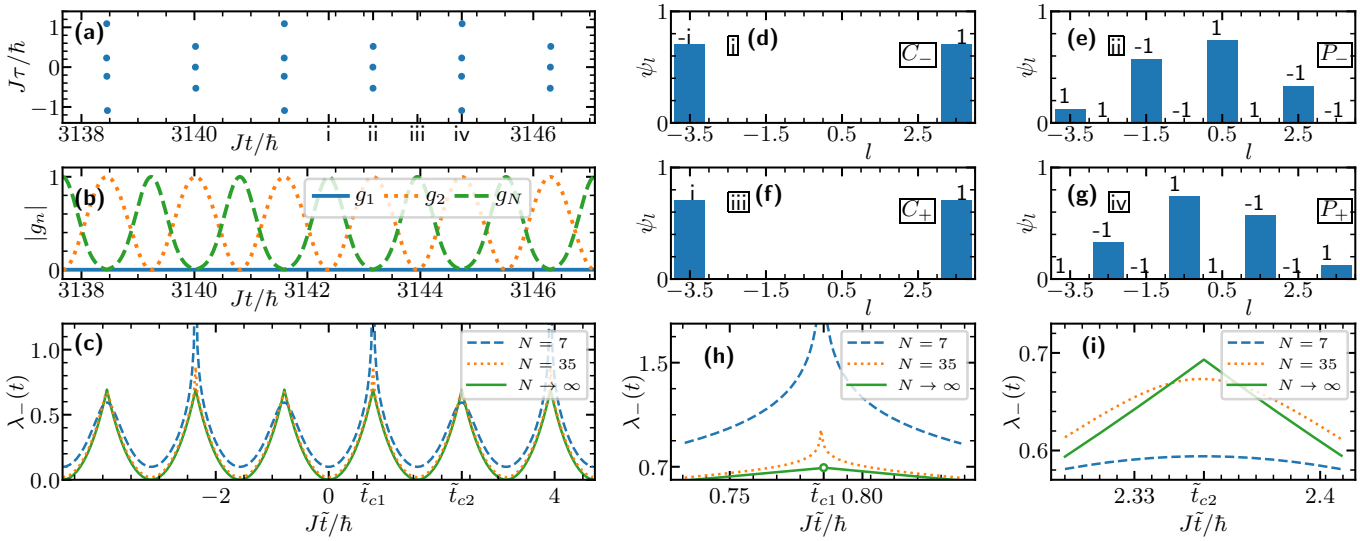

FIG. 4. (color online) (a,b) Zeros of $G(z)$ in the complex plane of time for 7 particles and the corresponding normalized correlation functions. (d-g) The wave functions at four times picked up from (a). (c) The rate function $\lambda_-(t)$. (h) and (i) show details of $\lambda_-(t)$ near t_c. The hollow dot in (h) represents the discontinuity of $\lambda_-(t)$ at $\tilde{t}_{c1}$ where it approaches infinity. In all panels U and J are fine tuned such that $|\psi(t^*)\rangle = |C_-\rangle$.

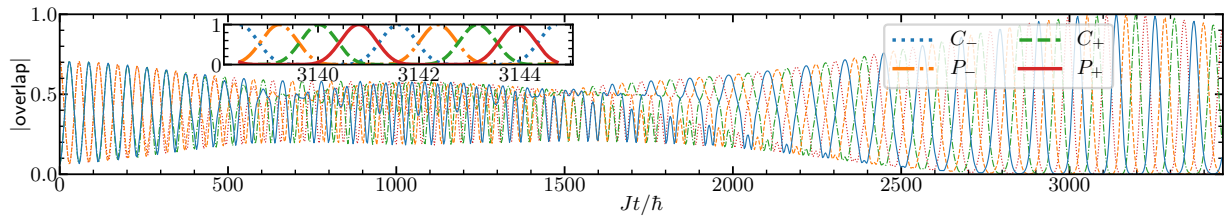

FIG. 5. (color online) The overlaps between the state $|\psi_t\rangle$ and four entangled states defined in the main text as a function of time. We have used $N = 8$ bosons and $U/J = 0.001$.

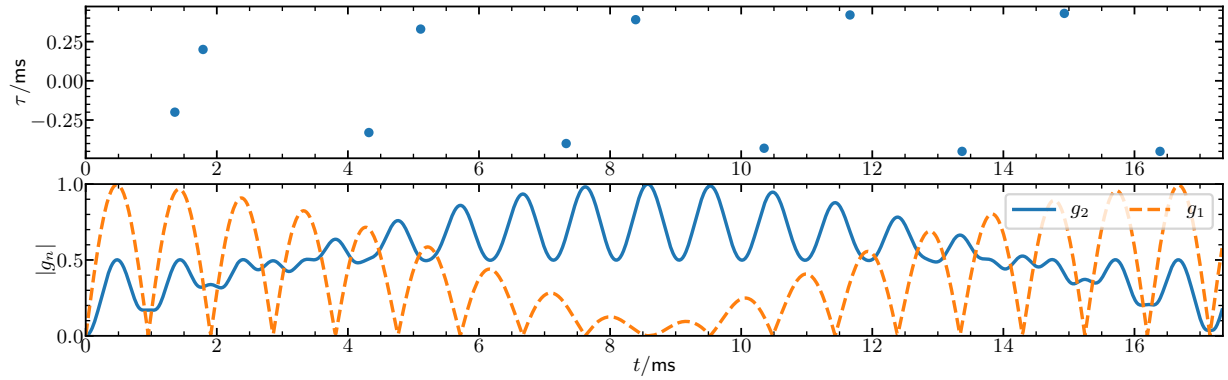

FIG. 6. (color online) Zeros of $G(z)$ in the complex plane and normalized correlation functions for 2 particles in optical tweezers. $U/J = 0.22$ and $J/2\pi = 262$Hz.

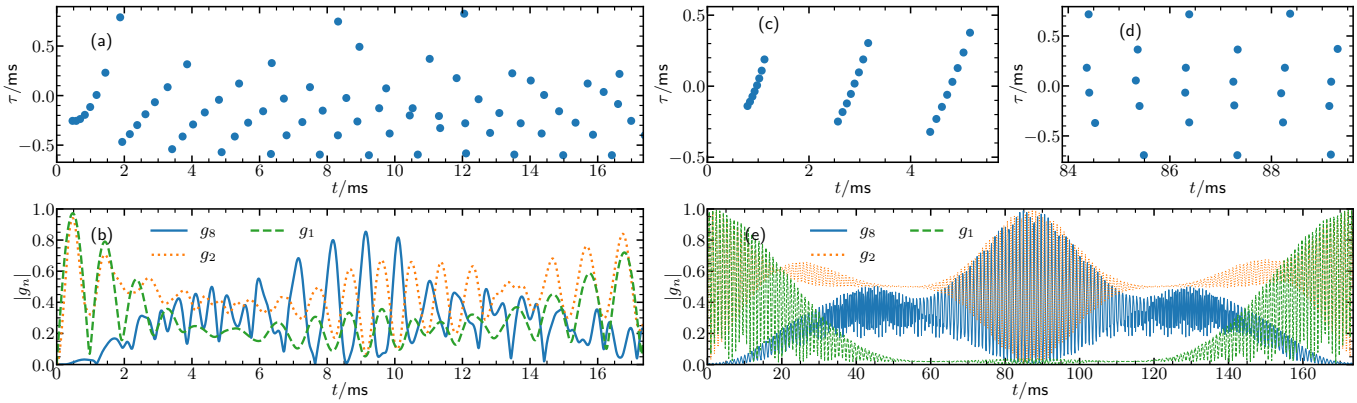

FIG. 7. (color online) (a,c,d) Zeros of $G(z)$ in the complex plane and (b,e) normalized correlation functions for 8 particles in optical tweezers. $J/2\pi = 262$Hz. (a,b) are for $U/J = 0.22$ and (c-e) are for $U/J = 0.022$.